

Home Search Collections Journals About Contact us My IOPscience

On-chip concentration of bacteria using a 3D dielectrophoretic chip and subsequent laserbased DNA extraction in the same chip

This content has been downloaded from IOPscience. Please scroll down to see the full text.

2010 J. Micromech. Microeng. 20 065010

(http://iopscience.iop.org/0960-1317/20/6/065010)

View the table of contents for this issue, or go to the journal homepage for more

Download details:

IP Address: 114.70.8.206

This content was downloaded on 01/04/2014 at 16:27

Please note that terms and conditions apply.

J. Micromech. Microeng. 20 (2010) 065010 (10pp)

On-chip concentration of bacteria using a 3D dielectrophoretic chip and subsequent laser-based DNA extraction in the same chip

Yoon-Kyoung Cho^{1,3}, Tae-hyeong Kim¹ and Jeong-Gun Lee²

E-mail: ykcho@unist.ac.kr

Received 13 January 2010, in final form 15 April 2010 Published 11 May 2010 Online at stacks.iop.org/JMM/20/065010

Abstract

We report the on-chip concentration of bacteria using a dielectrophoretic (DEP) chip with 3D electrodes and subsequent laser-based DNA extraction in the same chip. The DEP chip has a set of interdigitated Au post electrodes with 50 μ m height to generate a network of non-uniform electric fields for the efficient trapping by DEP. The metal post array was fabricated by photolithography and subsequent Ni and Au electroplating. Three model bacteria samples (*Escherichia coli*, *Staphylococcus epidermidis*, *Streptococcus mutans*) were tested and over 80-fold concentrations were achieved within 2 min. Subsequently, on-chip DNA extraction from the concentrated bacteria in the 3D DEP chip was performed by laser irradiation using the laser-irradiated magnetic bead system (LIMBS) in the same chip. The extracted DNA was analyzed with silicon chip-based real-time polymerase chain reaction (PCR). The total process of on-chip bacteria concentration and the subsequent DNA extraction can be completed within 10 min including the manual operation time.

S Online supplementary data available from stacks.iop.org/JMM/20/065010/mmedia

(Some figures in this article are in colour only in the electronic version)

1. Introduction

During recent decades, significant advances have emerged in the area of microTAS (μ TAS) to develop rapid, sensitive and user-friendly molecular assays suitable for medical diagnostics, pathogen detection, and food or water testing [1–8]. Among the many technologies available for biological sample concentration such as centrifugation, size- or affinity-based filtration, electrokinetic methods (electroosmosis, electrophoresis, and dielectrophoresis (DEP)), optical tweezers and magnetic manipulation, the electrokinetic methods could be a suitable solution to manipulate cells and particles on microchips thanks to the favorable scaling effects.

In DEP, the differences in polarizability between particles and solution in a non-uniform electric field give rise to a net force acting on the particle [9]. It has been particularly attractive because the DEP operations such as sorting or trapping of biological particles are electrically switchable and, unlike electrophoresis, non-charged particles can also be manipulated without significant movement of the fluid.

DEP force arises when a polarizable object is subjected to a non-uniform electric field and can be written to a first approximation as [10]

$$F_{\rm DEP} = \alpha(\omega) E_y \frac{\partial E}{\partial y} \tag{1}$$

where $\alpha(\omega)$ is the polarizability of the object at the angular frequency ω and y is the direction of the applied external field

¹ School of Nano-Biotechnology and Chemical Engineering, UNIST (Ulsan National Institute of Science and Technology) Banyeon-ri 100, Ulsan 689-798, Korea

² Bio & Health Group, Samsung Advanced Institute of Technology, PO Box 111, Suwon, 440-600, Korea

³ Author to whom any correspondence should be addressed.

E. For a spherical object of radius a, the DEP force is solved analytically in a form

$$F_{\text{DEP}} = 2\pi a^3 \varepsilon_m \text{Re} \left(\frac{\varepsilon_p^* - \varepsilon_m^*}{\varepsilon_p^* + 2\varepsilon_m^*} \right) \nabla E^2$$
 (2)

where ε_p^* and ε_m^* are the complex permittivity of the dielectric particle and the medium, respectively. Depending on the differences in the complex permittivity of the particle and the medium, the object may be either attracted to (p-DEP, positive DEP) or repelled from (n-DEP, negative DEP) the high field gradient region.

A number of studies have employed DEP for the mechanism of the separation and concentration of bacteria [10–16]. Selective capturing of specific target bacteria from the mixture of live and dead bacteria [13, 14] or different types of bacteria [11, 12, 16] has been demonstrated using alternating current DEP (ac-DEP). DEP has also been employed for the application of water monitoring, and it is desired to have devices that can handle a large volume of samples in a short time in order to have good sensitivity as well as a rapid analysis time for the bacteria detection [11, 12, 16].

We have developed a bacteria concentration and subsequent DNA extraction technique using a DEP chip with 3D electrodes. The concentrated bacteria was further investigated by on-chip cell lysis using laser irradiation [17], and then the extracted DNA was transferred to a separate silicon chip-based real-time PCR machine for further genomic analysis [18]. The bacteria concentration and DNA extraction could be completed within 10 min on a 3D DEP chip and 30 thermal cycles of real-time PCR could be completed within 20 min.

2. Design and fabrication of 3D dielectrophoretic chips

The majority of DEP studies reported in the literature employed 2D metallic electrodes, and the experiments have been carried out at a very slow flow velocity, e.g. $\sim 0.1 \text{ mm s}^{-1}$ [11, 19] or at no flow conditions. For example, it was reported that the DEP capture efficiency was decreased from 90% to 65% when the flow velocity was increased from 0.8 to 2.4 mm s⁻¹ [20]. Assuming that the cross-sectional area of the DEP chip is 0.3 mm², the flow velocity of 0.1 mm s⁻¹ corresponds to the flow rate of 1.8 μ L min⁻¹.

In the conventional 2D DEP chips using planar metallic electrodes, the DEP force rapidly decays as the distance from the electrodes increases, which results in poor capture efficiency, typically less than 20% for micron-sized bacteria at high flow velocities (>10 mm s⁻¹). This is one of the difficulties that have prevented DEP from being widely used in large volume applications.

Various kinds of electrode designs have been employed to increase the effective volume that could be under control of DEP forces. An example of the 3D DEP trap is the dielectric caging formed by octopole electrodes [21]. The negative DEP trap was formed in the middle of the flow channel by aligning

two glass electrode chips face to face. However, the cells could be trapped at flow rates only up to 0.05 mm s^{-1} [21].

In addition, an extruded quadrupole structure was employed to enhance the dielectric trapping forces [22]. The holding force using negative DEP was increased about five times compared to that of the octopole electrodes, in which micro beads with a particle diameter of 13 μ m were successfully trapped at flow rates up to 1.3 mm s⁻¹ [22]. Because the negative DEP mechanism was utilized, the metal wires exposed on the bottom surface have adverse effects on the holding force.

Park *et al* fabricated a 3D high-aspect-ratio carbon structures using carbon microelectromechanical systems and used for purification of canola oil with carbon nano fiber contamination [23]. The importance of 3D electrode design was addressed together with the electric and velocity field simulations of 2D versus 3D electrodes.

Iliescu *et al* reported separating particles using a DEP chip with asymmetric electrodes under continuous flow [24, 25]. An asymmetric 3D electrode consists of rows of thin and thick pillars with square cross-section. As a result, it generated an increased gradient of the electric field in the vertical plane. This phenomenon helped particles experiencing negative DEP to levitate easily.

Bidirectional field-flow particle separation was demonstrated by using a DEP chip with 3D electrodes [26]. After the separation of particles in different locations in the chip, one population is first collected by flowing a buffer solution. Then, the other population is collected at the second outlet by flowing a buffer in the perpendicular direction. The device has been tested successfully with the mixture of viable and non-viable yeast cells [26].

In addition, a 3D DEP filtering chip utilizing silica beads between two parallel plate electrodes was introduced for continuous flow separation at relatively high flow rates, e.g. 0.1 mL min⁻¹. The particles with positive DEP characteristics could be trapped around the contact points between the silica beads because it is the place showing the highest electric field gradients. However, the particles with negative DEP properties were repelled into the space between the beads [27, 28]. This could increase the handling volume and speed of the process. However, the non-uniformity of the particles may affect the reproducibility of the experiments and relatively high voltage, e.g. 200 V, was required [27, 28].

Moreover, Iliescu *et al* suggested a 3D DEP chip whose microchannel walls were made of heavy-doped silicon so that they could also function as electrodes to generate 3D DEP force [29–32]. In the undulating microchannel wall shape, the particles with the negative DEP properties were trapped in the fluidic dead zones, while the particles with positive DEP properties were concentrated in the regions where the fluidic velocity as well as the electric field gradients was the highest. Sequential field-flow cell separation was possible by first increasing flow velocity to remove the particles with positive DEP forces and then by removing the electric field to flow out the particles with negative DEP forces [29–32].

Wang et al also fabricated a set of interdigitated electrodes in the sidewall of the microchannels and used it to generate non-uniform electrical fields so that the negative DEP forces can repel the beads or cells from the sidewalls. A countering DEP force is generated from another set of electrodes patterned on the opposing sidewall. These lateral negative DEP forces can be adjusted by the voltage and frequency applied. By manipulating the coupled DEP forces, the particles flowing through the microchannel can be positioned at different equilibrium points along the width direction and continue to flow into different outlet channels [33]. However, this geometry is more appropriate for continuous separation, not for trapping- and release-type devices for particle concentration.

Hoettges *et al* developed a nonconventional DEP device using 3D well structure, similar in size and pitch to typical microtiter well plate, but having electrodes along the inner surface of the well in order to be used in high-throughput screening and rapid assay applications. The 3D electrodes structures inside of the well was fabricated by drilling a plates constructed by laminating 12 layers of 17 μ m thick copper electrodes and 75 μ m thick polyimide [34].

More recently, Cetin *et al* introduced a 3D DEP device utilizing two asymmetric 3D copper electrodes that were embedded inside the microchannel along the wall [35]. The soft-lithography-type fabrication methods were relatively simple and inexpensive, and the continuous separation of particles with different sizes was demonstrated.

In addition, Gonzalez *et al* demonstrated a ratchettype DEP device for particle analysis [36]. The electrodes fabricated by electroforming methods acted as the wall of the microchannel as well.

In this paper, we have developed a 3D DEP chip with interdigitated electrodes for a rapid cell concentration. The device has a series of the electroplated 3D electrodes fabricated by photolithography and electroplating technologies. The particle trapping by p-DEP occurs in the space between the Au post electrodes located in the interdigitated form. The capture efficiency and the concentration ratio have been systematically evaluated using three model bacteria samples (*Escherichia coli, Staphylococcus epidermidis, Streptococcus mutans*) as a function of flow velocities up to 42 mm s⁻¹.

3. Materials and methods

3.1. Cell preparation and quantification of bacterial genomic DNA by real-time PCR

A Gram-negative bacteria, *E. coli* (ATCC# 11775), and two Gram-positive bacteria, *S. epidermidis* (ATCC# 14990) and *S. mutans* (ATCC# 35668), were used. *E. coli* and *S. mutans* were grown in BHI (brain heart infusion) broth (BD, USA) at 37 °C and *S. epidermidis* was grown in nutrient broth (BD, USA) at 27 °C and 37 °C, respectively. The cells were harvested after 18 h, washed three times with phosphate-buffered saline (PBS) washing buffer and the final concentration was adjusted to an optical density (OD) of 1.0 at 600 nm.

For the visualization of the cells under a fluorescence microscope, bacteria were stained using a live/dead BacLight Bacterial viability kit (Molecular Probes, USA) according to the manufacturer's instruction. SYTO 9 penetrates the bacteria membranes and stains the cells green, while propidium iodide only penetrates cells with damaged membranes, and the combination of the two dyes makes the bacteria red. The concentration of the bacteria was measured either by the plating method using 3M colony paper or by using a fluorometer (Thermo Scientific Fluoroskan Ascent, FL, USA) depending on the initial cell concentration.

For the quantification of the bacterial DNA, DNA extraction from the concentrated bacteria solution in the 3D DEP chip was performed by using the laser-irradiated magnetic bead system (LIMBS) [17]. After the lysis step of the laser irradiation for 30 s, the magnetic beads were driven to one side using the permanent magnet, and the DNA solution was taken out and followed by the real-time PCR detection. A pair of primers (5'-TGTATGAAGAAGGCTTCG-3' and 5'-AAAGGTATTAACTTTACTC-3') and TaqMan probes (FAM-5'-TGTATGAAGA and AGGCTTCGGGTTGTAAA GTACTTTC-AGCGGGGAGGAAGGGAGTAAAGTTAATA CCTTT-3'-TAMRA) were used for the real-time PCR. These are complementary to each end of a gene encoding the 16S ribosomal RNA, allowing the amplification of its entire coding region. The amplicon size was 70 bp. PCR amplification was carried out using Taq polymerase (Solgent, Korea) for 30 cycles (95 °C for 2 min to pre-denature, 95 °C for 15 s to denature, 58 °C for 30 s to anneal and extend). The PCR was performed by real-time PCR (TMC 1000, SAIT, Korea) [18] with a total volume of 1 μ L reaction mixture containing 10× PCR buffer (2.5 mM MgCl₂, Solgent. Co. Ltd, Korea), $0.9 \mu M$ of forward and reverse primers, and also $0.4 \mu M$ of TaqMan probe (Bioneer, Korea), 200 μ M dNTP mixture and 0.1 U μ L⁻¹ Taq polymerases (Solgent, Korea).

3.2. Design of microfluidic and electric interface jig for DEP operation

A custom-built microfluidic and electric interface jig as shown in figure 1(A) was used to introduce cell solution into the chip, apply the electric field and visualize the bacteria trapping. The DEP chip is located on the jig that is designed to fit into the inverted microscope (Eclipse TE300, Nikon, Japan). The interface jig made of Plexiglas was aligned on top of the DEP chip and clamped tightly. It was designed to minimize the dead volume and the contamination using the NanoPort assemblies (N-126H, Upchurch, USA). Fluids were introduced into the chip from 3 mL syringes via 0.010 inch ID tubing (1581, Upchurch, USA) using a syringe pump (PHD 2000, Harvard, USA). Both the tubing and the chips are disposable.

The electric contacts to the DEP chip were made by using Leeno pins, which are connected to a function generator (33120A, Agilent, USA) through the BNC connectors. Sinusoidal waveforms at 20 Vpp at various frequencies raging from 100 Hz to 10 MHz were applied. Phase-contrast and fluorescence images of the bacteria were taken using a cooled CCD camera (Quantix 57, Photometrics, USA) attached to an inverted microscope (Eclipse TE300, Nikon, Japan).

Before the bacteria solution was introduced into the chip, the system was flushed with 1–3 mL of the media with

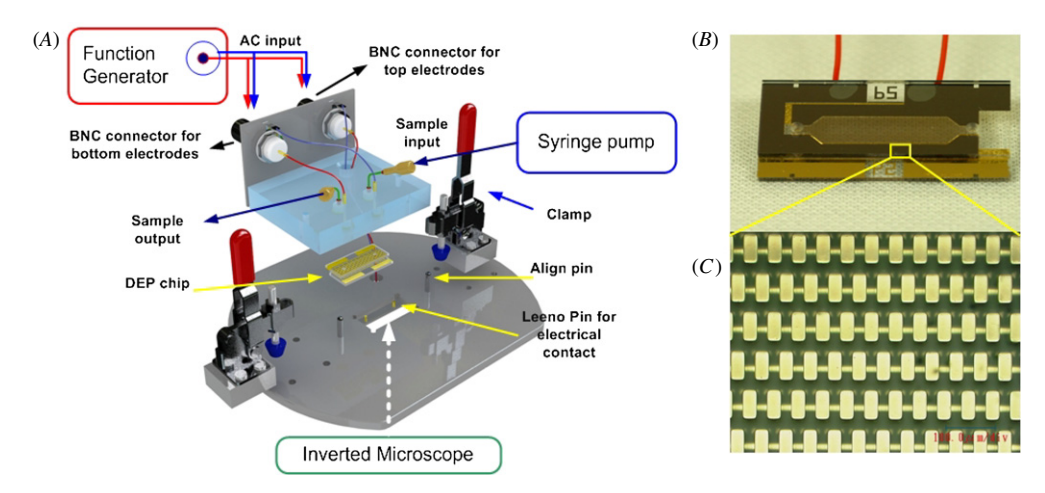


Figure 1. (A) Schematic diagram of the microfluidic and electric interface jig. The bottom stage is designed to fit onto an inverted microscope. The tubing and the DEP chips are disposable. A fluidic interface jig was designed to minimize the device's internal dead volume. An electric connection between the chip and the BNC connector was made by using Leeno pins. (B) The DEP chip was assembled by using a double-sided adhesive tape. The tape has a chamber pattern and forms a fluidic chamber with a volume of 3.5 μ L. The photo image shows the assembled chip. (C) The optical micrograph shows the Au electrode arrays.

the same conductivity as the bacteria solution for priming. The bacteria solution was introduced into the chip at various flow rates ranging from 50 to 500 μ L min⁻¹ and monitored with the microscope. The experimental results are compared at the same flow rates. However, the flow velocities are also described because the effective contact area is different depending on the chip types. The flow rate of 100 μ L min⁻¹ in our devices corresponds to flow velocities of 6.2 mm s⁻¹ and 8.4 mm s⁻¹ for 2D DEP and 3D DEP chips, respectively.

3.3. Chip fabrication

The DEP chip was made of glass patterned with gold electrodes as shown in figure 1(B). Two glass chips are assembled together by using a patterned 3M double-sided adhesive tape (thickness was 90 μ m, 7953 MP). The fluidic chamber was formed by using the patterned adhesive tape. In the current experiments, the chamber width was 3 mm, the length was 10 mm and the depth was 90 μ m. The fluid volume in the chamber was 3.5 μ L including the volume of inlet holes. The optical microscope image of the DEP chip is shown in figure 1(C).

Figure 2(*A*) shows the fabrication process of the 3D DEP trap. It essentially involves electroplating Ni (50 μ m) into a photoresist (PR) (70 μ m) mold followed by the PR removal and Au (0.5 μ m) electroless plating. A glass wafer (4" diameter, 1 mm thick, Corning Pyrex® 7740) was cleaned by the piranha solution (H₂SO₄:H₂O₂ = 1:1, 110 °C) for 10 min and baked at 100 °C in an oven for 10 min. Titanium (100 Å) and gold (1000 Å) layers were deposited on the glass substrate by thermal evaporation (A Tech Co. Ltd, Korea) and patterned to form the bottom seed electrode. The chips prepared at this stage are used for the 2D DEP experiments.

For 3D DEP chips, an additional SiO_2 passivation layer (5000 Å) was deposited by PECVD (STS 310PC, UK). Then, the 70 μ m thick positive photoresist (AZ 9260, Clariant Ltd, USA) pattern was formed on the SiO_2 passivation layer as

a SiO₂ etch mask and mold for self-aligned 3D DEP trap electrodes electroplating [37, 38]. The SiO₂ layer was etched by buffered oxide etch (BOE, JT Backer®), and Ni plating is done until the photoresist mold was filled to reach a 50 μm thickness. The detailed experimental conditions of the Ni plating were previously described [37, 38]. Next, the photoresist mold was removed by acetone and treated on Ni etchant (HNO₃:DI = 1:3) for 1 min to remove Ni residues and improve the Ni surface for Au electroless plating. Finally, Au displaced the Ni surface when the Ni 3D DEP array was immersed in the electroless plating solution (Electroless FX-3 Make-up solution + potassium gold cyanide (PGC), CNC technology, Korea) at 85 °C for 10 min. Figure 2(B) shows the SEM image of the fabricated Au post array with the dimensions of the Au post and the electrode connection lines. The trapping site by positive DEP is located in interdigitated form as schematically shown in figure 2(C). In the previously reported 3D DEP chips in which the sidewalls are also actively used as electrodes (figure 2(D)), the particle trapping region is located where the flow rate is also maximum [29–32]. However, in our geometry, the trapping site by p-DEP is located in the interdigitated form to enhance the trapping efficiency at high flow rate conditions.

4. Results and discussion

4.1. Frequency effect on the DEP of bacteria samples

The effect of the frequency on the DEP has been investigated using three model bacteria samples. For example, the *S. epidermidis* solution (10^5 cells μL^{-1} , the media conductivity was 2.0 mS m⁻¹) was introduced with the flow rate of 3 μ L min⁻¹ (flow velocity of 0.19 mm s⁻¹) and the real-time images were captured by the inverted microscope equipped with a cooled CCD camera. The series of captured images were analyzed with image analysis software (Metamorph V.6.1), and the fluorescence intensity

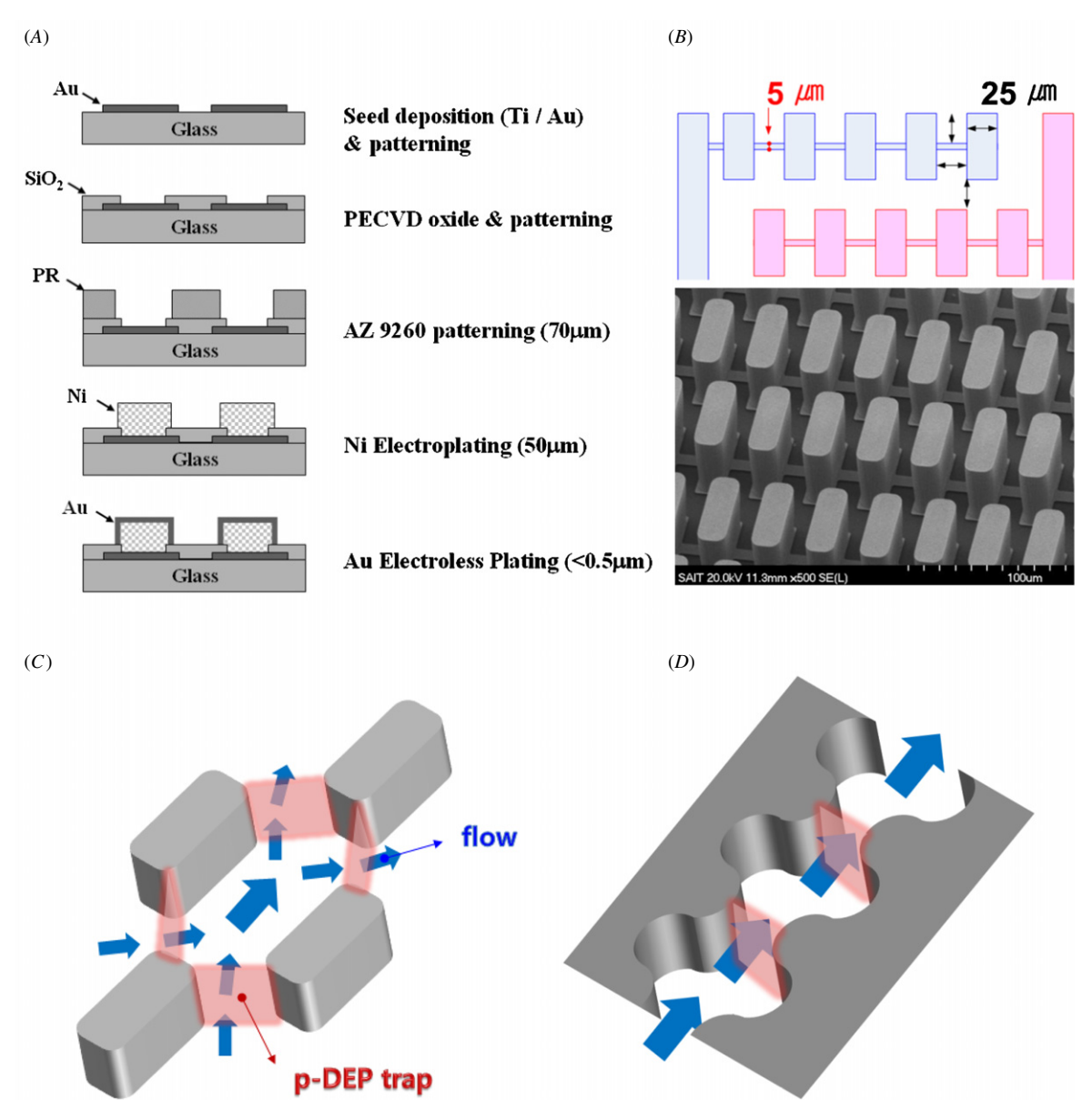


Figure 2. (A) Fabrication process of the Au post arrays for the 3D DEP trap. It essentially involves electroplating Ni (50 μ m) into a photoresist (PR) (70 μ m) mould followed by the PR removal and Au (0.5 μ m) electroless plating. (B) SEM image of the fabricated Au post array and schematic diagram showing the dimension of the Au electrodes. The connection line on the bottom has the width of 5 μ m and the distance between counter electrodes, D, and neighbor electrodes with same polarity, P, is all 25 μ m. The Au post has a width of 25 μ m, a length of 55 μ m, and a height of 50 μ m. (C) Schematic diagram showing the flow direction and the particle trapping location by positive DEP in the interdigitated 3D post arrays. (D) 3-D electrode walls [29–32].

was measured as a function of time. A planar-type castellated electrode was used, and the distance between electrodes with opposite polarities was 15 μ m. A sinusoidal electric field (10 Vpp) at different frequencies raging from 1 kHz to 10 MHz was applied for 1 min and removed. As shown in figure 3(A), the fluorescence intensity increased when the electric field was applied and decreased when the electric field was removed. In the case of the *S. epidermidis* solution with the media conductivity of 2.0 mS m⁻¹, the positive DEP was observed between 100 kHz and 10 MHz.

As shown in figure 3(B), the maximum fluorescent intensities measured 1 min after the electric field was applied were compared as a function of frequency. In the case of

E. coli, the maximum positive DEP trapping was observed at 1 MHz while both Gram-positive bacteria S. epidermidis and S. mutans showed maximum trapping at 300 kHz. The maximum positive trapping frequency of 1 MHz for E. coli is in good agreement with the previous papers [39–43]. The maximum positive trapping frequency depends on the dielectric properties, e.g. dielectric permittivity and electric conductivity of cytoplasm and the membrane, of each bacterium [43].

When we carried out experiments with a 1:1 mixture of live and dead *E. coli*, only live *E. coli*, shown in green, were selectively trapped at frequencies between 5 MHz and 15 MHz. On the other hand, only dead bacteria, shown

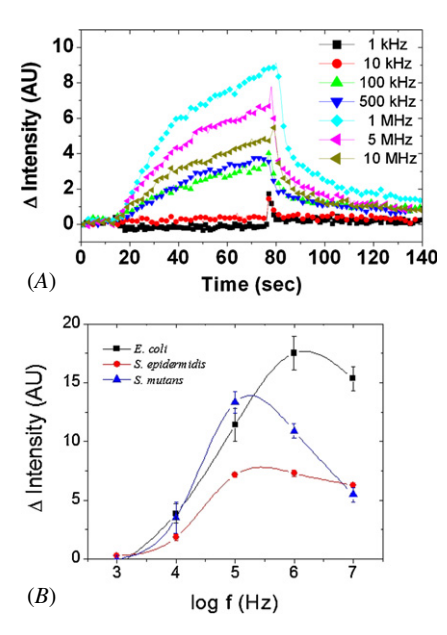


Figure 3. Characterization of the DEP properties of the bacteria solution. (*A*) Fluorescence intensity increased when the electric field was applied and decreased when the electric field was removed. For the case of the *S. epidermidis* solution with the media conductivity of 2.0 mS m⁻¹, the positive DEP was observed between 100 kHz and 10 MHz. (*B*) The maximum fluorescent intensity measured at 1 min after the DEP trap of each bacteria solution (10^5 cells μ L⁻¹, the media conductivity was 0.5 mS m⁻¹) was compared as a function of frequency.

in red, were trapped at the frequencies between 1 kHz and 10 kHz. Between 100 kHz and 1 MHz, both live and dead bacteria are trapped and the image is shown in yellow (see supplement 1) in stacks.iop.org/JMM/20/065010/mmedia.

4.2. Quantitative measurement of the capture efficiency

Figures 4(*A*) and (*B*) show the optical images of 2D DEP and 3D DEP chips, respectively, obtained after 2 min of applying a sinusoidal electric field of 20 Vpp at 1 MHz when the *E. coli* solution (0.1 OD, 5–10 × 10⁴ cells μ L⁻¹, 0.5 mS m⁻¹) flowed with a flow rate of 250 μ L min⁻¹ (flow velocity was 15.4 mm s⁻¹ and 21.4 mm s⁻¹ for 2D DEP and 3D DEP chips, respectively). It is clear that a much larger number of bacteria were trapped in the 3D DEP chip compared to the 2D DEP chip (see also the movies shown in stacks.iop.org/JMM/20/065010/mmedia).

One simple method to measure the capture efficiency could be to use fluorescence intensities of the images taken under the fluorescence microscope [12, 13, 44]. The capture efficiency could be calculated from the ratio of the fluorescence intensity of the images taken before and after the electric field was applied. However, the fluorescence intensity of the images taken when the electric field is not applied is very small especially when a very dilute sample is used. Therefore, small differences in the denominator signal could generate a big error on the estimation of the concentration efficiency.

For better quantitative measurement of the capture efficiency, we have used non-labeled bacteria and measured the bacteria concentration of three samples at each experiment; initial cell suspension $(I_{\rm ini})$, control sample obtained by flowing the cell suspension through the chip without applying the electric field $(I_{\rm OFF})$ and the solution flowing out of the chip when the DEP trapping is active $(I_{\rm ON})$. The real capture efficiency may vary as a function of time and the number of bacteria precaptured on the electrodes. However, for practical purposes, we have defined the apparent capture efficiency by the following equation:

Capture efficiency (%) =
$$(I_{\text{ini}} - I_{\text{ON}})/I_{\text{ini}} \times 100$$
. (3)

The concentration of the control sample obtained when the electric field was not applied, $I_{\rm OFF}$, was the same as the initial sample, $I_{\rm ini}$, within the experimental error range (CV% was less than 10%). Therefore, it was assumed that there was no significant nonspecific adsorption of bacteria on the DEP chips. In addition, the DEP operation in our experiments did not cause irreversible damage to bacterial cells in terms of cell viability.

As shown in figures 4(A) and (B), even though the bacteria were not fluorescently labeled, the trapped bacteria were clearly visible under the optical microscope because the local concentration was high. *E. coli* are trapped and formed the so-called pearl chain in the highest electric field gradient region.

Figure 4(C) shows the capture efficiency of E. coli flowing at the flow rate of 250 μ L min⁻¹. The capture efficiency of 20% for the 2D DEP chip was significantly enhanced to 50% for the case of 3D DEP chips with the electrode height of 50 μ m. It was further increased to about 80% when the top glass substrate was replaced by the chip with a planar-type electrode. It is expected to have better capture efficiency if 3D DEP chips are used for both top and bottom electrodes. With the same channel height of 90 μ m, however, we could not use 3D DEP chips for both top and bottom electrodes because it results in electrical contacts.

In figure 4(D), the concentration ratio after 2 min of applying the electric field is plotted as a function of the flow rate. The solid line is the predicted concentration ratio assuming 100% of the capture efficiency. The electric field condition to have maximum positive DEP force, e.g. 20 Vpp, 1 MHz for *E. coli* and 300 kHz for *S. mutans* and *S. epidermidis* was applied for 2 min. The concentration ratio was increased up to about 80 at about flow velocities of 16 mm s⁻¹.

In the case of *E. coli*, the concentration ratio was further increased at higher flow velocities but the slope was diminished suggesting that the capture efficiency was decreased. On the other hand, the concentration ratio was not further increased (*S. mutans*) or even decreased (*S. epidermidis*) at high flow velocities ($>20 \text{ mm s}^{-1}$). This suggests that no more bacteria could be captured or even previously trapped bacteria are released for *S. mutans* and *S. epidermidis*, respectively at high flow velocities ($>20 \text{ mm s}^{-1}$). The DEP force is usually smaller for Gram-positive bacteria than the Gram-negative bacteria.

The Joule heating could be ignored in our experimental conditions of 0.5–2.0 mS m⁻¹. In addition, it is worth mentioning that the geometry of electrodes that can provide the same DEP force at a lower value of the applied voltage could be advantageous due to its reduced Joule-heating effects. For

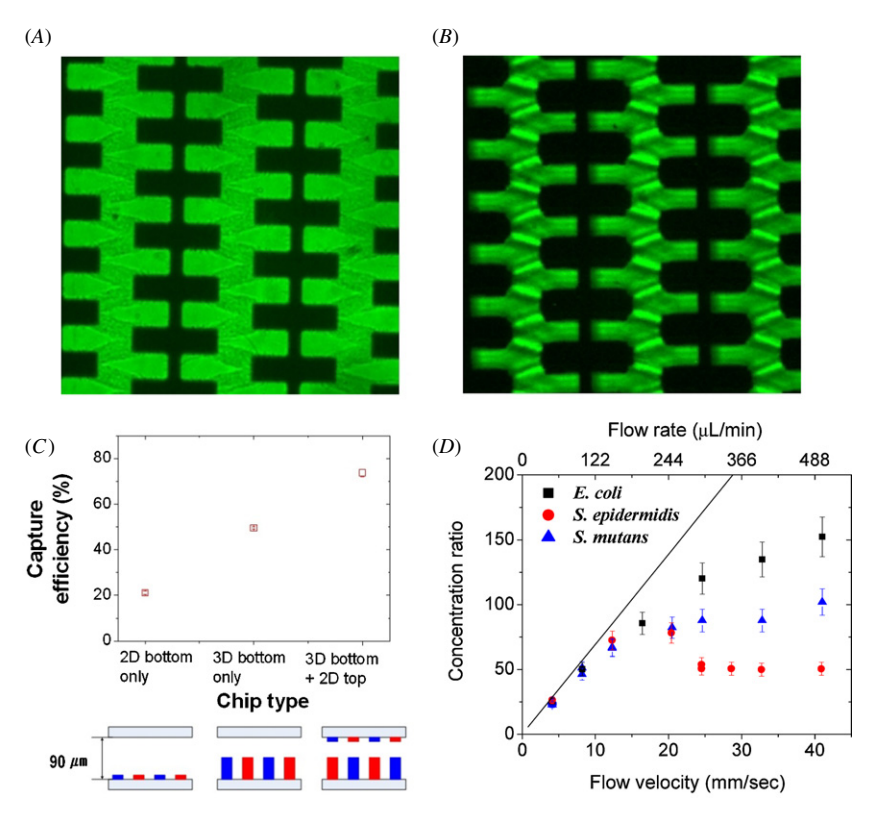


Figure 4. Differential interference contrast (DIC) microscope image of *E. coli* trapped by positive DEP. Optical microscope images of the 2D DEP chip (*A*) and 3D DEP chip (*B*) obtained 2 min after applying a sinusoidal electric field of 20 Vpp at 1 MHz when the *E. coli* solution (0.1 OD, 5–10 × 10⁴ cells μ L⁻¹, 0.5 mS m⁻¹) flowed with a flow rate of 250 μ L min⁻¹. (*C*) Capture efficiency of *E. coli* depending on the electrode dimension of the DEP chip. A sinusoidal electric field of 20 Vpp and 1 MHz was applied for 2 min when the *E. coli* solution (0.1 OD, 5–10 × 10⁴ cells μ L⁻¹, 0.5 mS m⁻¹) flowed with a flow rate of 250 μ L min⁻¹. (*D*) The concentration ratio, the concentration after 2 min of DEP operation divided by the initial concentration, is plotted as a function of the flow rate. The solid line is for the predicted value assuming 100% of the capture efficiency. Each of the data points is the average of three independent measurements.

example, Tay *et al* reported that the temperature increase in the 3D DEP device was 8–10 times lower than the conventional DEP device with planar electrodes [31].

4.3. Rapid concentration of bacteria and on-chip DNA extraction

On-chip DNA extraction from the bacteria captured by DEP has been previously demonstrated by osmotic shock in the microfluidic chip [15] or by electrolysis, i.e. applying pulses of high electric fields [45] or by introducing the lysis buffer solution [46]. However, the DNA extraction from Grampositive bacteria, which are known to be difficult to disrupt with other commonly used methods, has not been fully investigated.

We previously reported a novel cell lysis method, LIMBS [17]. The addition of magnetic beads to the pathogen-containing solution accelerated the heating speed upon laser irradiation. Therefore, DNA from various types of pathogens including both Gram-negative and Gram-positive bacteria was effectively extracted by simply applying 40 s of laser (808 nm, 1.0 W) irradiation.

In this paper, the rapid concentration of Gram-positive bacteria in the 3D DEP chip followed by on-chip cell lysis using LIMBS has been demonstrated. The concentration of the bacteria solution was achieved by flowing the dilute *S. mutans* solution (0.01 OD, $3-5 \times 10^3$ cells μL^{-1} , 0.5 mS m⁻¹) with a flow rate of 100 μL min⁻¹ for 4 min through the 3D DEP chip. The trapped bacteria are visible in the optical microscope image as shown in figure 5(A).

In order to obtain DNA from the concentrated bacteria using the LIMBS method, it was necessary to have uniformly dispersed magnetic beads inside of the chip. It was observed that the magnetic beads (Dynabeads® MyOneTM carboxylic acid, diameter = 1 μ m, Invitrogen) were also captured by positive DEP in the similar frequency ranges, from 100 kHz to 1 MHz, as the bacteria solution as shown in figure 5(*B*). Therefore, the magnetic beads were also captured by positive DEP when the diluted magnetic bead solution (1 μ g μ L⁻¹) was flowed with a flow rate of 50 μ L min⁻¹ for 1 min. Figure 5(*C*) shows the magnetic beads trapped by positive DEP.

The DEP trapping force of magnetic beads was observed to be smaller than that obtained when trapping bacteria. If the magnetic beads were trapped prior to the bacteria trapping, the pre-captured beads were flushed away when the bacteria solution was introduced with higher flow rate (e.g. 250 μ L min⁻¹). If the bacteria solution is introduced at flow rate less than 50 μ L min⁻¹, the previously captured magnetic beads were not released.

After the concentration of both bacteria and magnetic particles, the 3D DEP chip was transferred to the hand-held

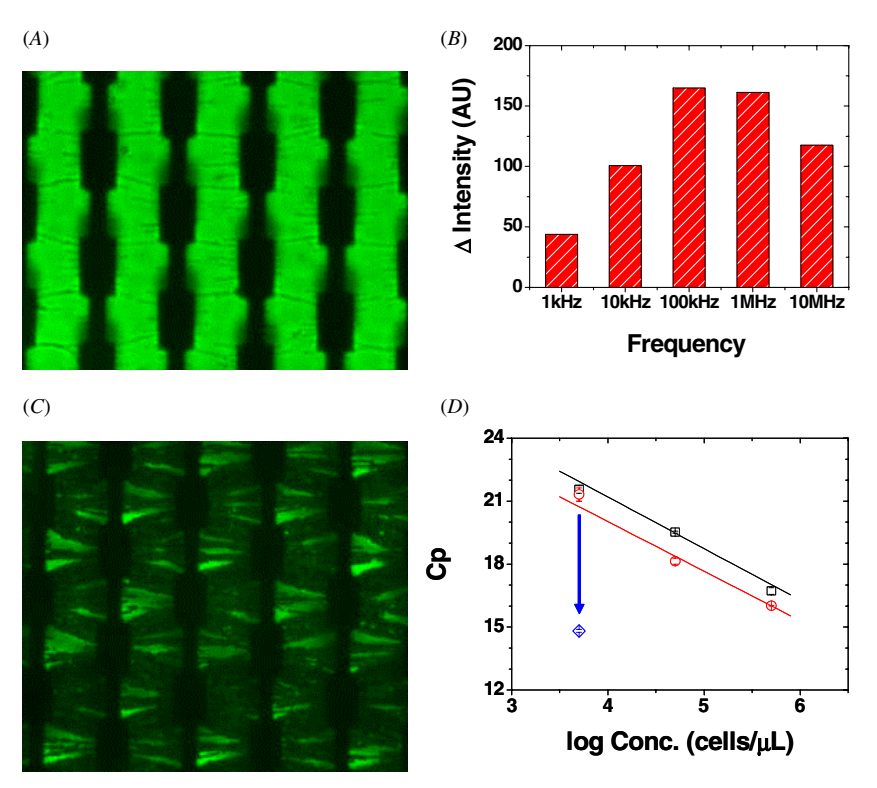


Figure 5. (A) Optical microscope image acquired after flowing the *S. mutans* solution (0.01 OD, $3-5 \times 10^3$ cells μL^{-1} , 0.5 mS m⁻¹) with a flow rate of 100 μ L min⁻¹ for 4 min. (B) Positive DEP was observed for the magnetic beads (100 μ g μL^{-1} , 7-12×10⁷ beads μL^{-1} , Dynabeads MyOne carboxylic acid, diameter = 1 μ m, Invitrogen) between 1 kHz and 10 MHz. (C) Optical microscope image taken after flowing the diluted magnetic bead solution (1 μ g μL^{-1}) with a flow rate of 50 μ L/min for 1 min in addition to the bacteria trap. (D) Real-time PCR results show that over 100 times concentration was achieved by using the 3D DEP chips (rhombus). The 3D DEP chips with Au post arrays (circles) showed better DNA extraction efficiency (smaller Cp values) than the silicon-glass bonded chips (squares).

LIMBS system [17]. After applying laser (808 nm) irradiation for 40 s, 2 μ L of extracted DNA solution was transferred to a separate silicon chip for the following chip-based real-time PCR analysis. The detailed performance of the silicon chip-based real-time PCR has been previously reported elsewhere [18, 47].

As shown in figure 5(D), the real-time PCR results show that about 100 times concentration was achieved by using 3D DEP chips. The bacteria concentration using the 3D DEP chip decreased cross point (Cp) value from 21.32 ± 0.31 to 14.82 ± 0.07 when the initial cell concentration was 3–5 \times 10^3 cells μL^{-1} (0.01 OD). The Cp is defined as the cycle number at which the fluorescence passes the fixed threshold. It has been reported that ten-fold differences in the template DNA concentration results in 3.32 cycle differences in Cp when PCR efficiency is 100% [18, 48]. It is also noteworthy that the 3D DEP chips with Au post arrays showed better DNA extraction efficiency (smaller Cp values) than the siliconglass bonded chips possibly because the laser energy is more effectively absorbed by the metal post arrays. The total process of the concentration of bacteria and the DNA extraction using LIMBS could be done on a 3D DEP chip within 10 min including manual chip transfer time. With 30 thermal cycles of PCR using the previously reported silicon chip-based real-time PCR machine [18], the total process of bacteria concentration, DNA extraction and PCR analysis could be completed within 30 min.

5. Concluding remarks

Though DEP has been used for the separation and concentration of various particles, rapid concentration and large volume application have not been fully elucidated. In this paper, 3D DEP chips with metallic post arrays have been designed and used for the rapid concentration of three model bacteria at high flow rates (>100 μ L min⁻¹). When the *E. coli* solution flows with the flow rate of 250 μ L min⁻¹, the capture efficiency of 20% for the 2D DEP chip was increased up to 80% for the 3D DEP chip. Over 80-fold concentration was achieved within 2 min at the flow velocity of 16 mm s⁻¹.

Furthermore, on-chip DNA extraction from the Grampositive bacteria captured by 3D DEP has been investigated using the laser-based cell lysis method [17]. A rapid concentration of both magnetic beads and bacteria was achieved by using postive DEP at the same frequency range. The real-time PCR results demonstrated that a DNA concentration enhancement of about 100 times could be achieved.

In conclusion, a rapid concentration of bacteria and onchip DNA extraction could be achieved using 3D DEP chips within 10 min. The extracted DNA could be directly used for the silicon chip-based real-time PCR for further genomic analysis. Compared to the current culture-based methods, the proposed 3D DEP chip-based method could provide benefits of enhanced detection sensitivity as well as rapid detection time for the water analysis to detect pathogens.

Acknowledgments

The authors gratefully acknowledge Dr Kak Namkoong, Dr Joonho Kim, Dr Jun-Bo Yoon and Dr Christopher Ko for helpful discussions and Byung Chul Lee, Seongyoung Jung and Jin-sung Park for conducting some parts of the experiments. This work was partially supported by the WCU (World Class University) program (R32-2008-000-20054-0) and the International Cooperative Program (2009-50245) through the National Research Foundation of Korea funded by the Ministry of Education, Science and Technology.

References

- [1] Whitesides G M 2006 The origins and the future of microfluidics *Nature* 442 368–73
- [2] Yager P, Edwards T, Fu E, Helton K, Nelson K, Tam M R and Weigl B H 2006 Microfluidic diagnostic technologies for global public health *Nature* 442 412–8
- [3] Auroux P A, Jossifidis D, Reyes D and Manz A 2002 Micro total analysis systems. 2. Analytical standard operations and applications (review) Anal. Chem. 74 2637–52
- [4] Burns M A 2002 Everyone's a (future) chemist *Science* **296** 1818–9
- [5] Knight J 2002 Microfluidics: Honey, I shrunk the lab *Nature* 418 474–5
- [6] Reyes D, Iossifidis D, Auroux P A and Manz A 2002 Micro total analysis systems: I. Introduction, theory, and technology (review) Anal. Chem. 74 2623–36
- [7] Vilkner T, Janasek D and Manz A 2004 Micro total analysis systems. Recent developments Anal. Chem. 76 3373–86
- [8] Cho Y K, Lee J G, Park J M, Lee B S, Lee Y and Ko C 2007 One-step pathogen specific DNA extraction from whole blood on a centrifugal microfluidic device *Lab Chip* 7 565-73
- [9] Pohl H A 1978 *Dielectrophoresis* (Cambridge: Cambridge University Press)
- [10] Chou C-F and Zenhausern F 2003 Electrodeless dielectrophoresis for micro total analysis systems *IEEE Eng. Med. Biol. Mag.* 22 62–7
- [11] Huang Y, Ewalt K L, Tirado M, Haigis R, Forster A, Ackley D, Heller M J, O'Connell J P and Krihak M J 2001 Electric manipulation of bioparticles and macromolecules on microfabricated electrodes *Anal. Chem.* 73 1549–59
- [12] Lapizco-Encinas B, Simmons B, Cummings E and Fintschenko Y 2004 Insulator-based dielectrophoresis for the selective concentration and separation of live bacteria in water *Electrophoresis* 25 1695–704
- [13] Lapizco-Encinas B H, Simmons B A, Cummings E B and Fintschenko Y 2004 Dielectrophoretic concentration and separation of live and dead bacteria in an array of insulators Anal. Chem. 76 1571–9
- [14] Li H and Bashir R 2002 Dielectrophoretic separation and manipulation of live and heat-treated cells of Listeria on microfabricated devices with interdigitated electrodes Sensors Actuators B 86 215–21

- [15] Prinz C, Tegenfeldt J O, Austin R H, Cox E C and Sturm J C 2002 Bacterial chromosome extraction and isolation Lab Chip 2 207–12
- [16] Yang J M et al 2002 An integrated, stacked microlaboratory for biological agent detection with DNA and immunoassays Biosens. Bioelectron. 17 605–18
- [17] Lee J-G, Cheong K H, Huh N, Kim S, Choi J-W and Ko C 2006 Microchip-based one step DNA extraction and the real-time PCR in one chamber for rapid pathogen identification *Lab Chip* 6 886–95
- [18] Cho Y-K et al 2006 Clinical evaluation of micro-scale chip-based PCR system for rapid detection of hepatitis B virus Biosens. Bioelectron. 21 2161–9
- [19] Becker F, Wang X, Huang Y, Pethig R, Vykoukal J and Gascoyne P 1995 Separation of human breast cancer cells from blood by differential dielectric affinity *Proc. Natl* Acad. Sci. USA 92 860–4
- [20] Yang L, Banada P P, Chatni M R, Lim K S, Bhunia A K, Ladisch M and Bashir R 2006 A multifunctional micro-fluidic system for dielectrophoretic concentration coupled with immuno-capture of low numbers of Listeria monocytogenes Lab Chip 6 896–905
- [21] Muller T, Gradl G, Howitz S, Shirley S, Schnelle T and Fuhr G 1999 A 3D microelectrode system for handling and caging single cells *Biosens. Bioelectron.* 14 247–56
- [22] Voldman J, Gray M L, Toner M and Schmidt M A 2002 A microfabrication-based dynamic array cytometer *Anal*. *Chem.* 74 3984–90
- [23] Park B Y and Madou M J 2005 3D electrode designs for flow-through dielectrophoretic systems *Electrophoresis* 26 3745–57
- [24] Iliescu C, Liming Y, Guolin X and Tay F E H 2006 A dielectrophoretic chip with a 3D electric field gradient *Microelectromech. Syst. J.* 15 1506–13
- [25] Iliescu C, Tresset G and Xu G 2009 Dielectrophoretic field-flow method for separating particle populations in a chip with asymmetric electrodes *Biomicrofluidics* 3 044104–10
- [26] Iliescu C, Yu L, Tay F E H and Chen B 2008 Bidirectional field-flow particle separation method in a dielectrophoretic chip with 3D electrodes Sensors Actuators B 129 491–6
- [27] Ciprian I et al 2007 Dielectrophoretic separation of biological samples in a 3D filtering chip J. Micromech. Microeng. 17 S128
- [28] Iliescu C, Xu G, Loe F C, Ong P L and Tay F E H 2007 A 3D dielectrophoretic filter chip *Electrophoresis* 28 1107–14
- [29] Ciprian I et al 2005 Fabrication of a dielectrophoretic chip with 3D silicon electrodes J. Micromech. Microeng. 15 494
- [30] Liming Y, Iliescu C, Guolin X and Tay F E H 2007 Sequential field-flow cell separation method in a dielectrophoretic chip with 3D electrodes *Microelectromech. Syst. J.* 16 1120–9
- [31] Tay F E H, Yu L M, Pang A J and Iliescu C 2007 Electrical and thermal characterization of a dielectrophoretic chip with 3D electrodes for cells manipulation *Electrochim. Acta* 52 2862–8
- [32] Iliescu C, Tresset G and Xu G 2007 Continuous field-flow separation of particle populations in a dielectrophoretic chip with three dimensional electrodes *Appl. Phys. Lett.* 90 234104–3
- [33] Wang X, Hofmann O, Das R, Barrett E M, deMello A J, deMello J C and Bradley D D C 2007 Integrated thin-film polymer/fullerene photodetectors for on-chip microfluidic chemiluminescence detection *Lab Chip* 7 58–63
- [34] Hoettges K F, Hubner Y, Broche L M, Ogin S L, Kass G E N and Hughes M P 2008 Dielectrophoresis-activated multiwell plate for label-free high-throughput drug assessment *Anal. Chem.* **80** 2063–8

- [35] Çetin B, Kang Y, Wu Z and Li D 2009 Continuous particle separation by size via AC-dielectrophoresis using a lab-on-a-chip device with 3D electrodes *Electrophoresis* 30 766–72
- [36] Gonzalez C F and Remcho V T 2009 Fabrication and evaluation of a ratchet type dielectrophoretic device for particle analysis J. Chromatogr. A 1216 9063–70
- [37] Yoon J-B, Kim B-I, Choi Y-S and Yoon E 2003 3D construction of monolithic passive components for RF and microwave ICs using thick-metal surface micromachining technology *IEEE Trans. Microw. Theory Tech.* 51 279–88
- [38] Yoon J-B, Han C-H, Yoon E and Kim C-K 1998 Novel and high-yield fabrication of electroplated 3D micro-coils for MEMS and microelectronics SPIE Conf. on Micromachining and Microfabrication Process Technology IV (Santa Clara, CA); Proc. SPIE 3511 233–40
- [39] Suehiro J, Hamada R, Noutomi D, Shutou M and Hara M 2003 Selective detection of viable bacteria using dielectrophoretic impedance measurement method J. Electrost. 57 157–68
- [40] Suehiro J, Zhou G, Imamura M and Hara M 2003 Dielectrophoretic filter for separation and recovery of biological cells in water *IEEE Trans. Ind. Appl.* 39 1514–21
- [41] Green N G, Morgan H and Milner J J 1997 Manipulation and trapping of sub-micron bioparticles using dielectrophoresis *J. Biochem. Biophys. Methods* **35** 89–102

- [42] Markx G H, Dyda P A and Pethig R 1996 Dielectrophoretic separation of bacteria using a conductivity gradient J. Biotechnol. 51 175–80
- [43] Holzel R 1999 Non-invasive determination of bacterial single cell properties by electrorotation *Biochim. Biophys. Acta* 1450 53–60
- [44] Lapizco-Encinas B H, Davalos R V, Simmons B A, Cummings E B and Fintschenko Y 2005 An insulator-based (electrodeless) dielectrophoretic concentrator for microbes in water J. Microbiol. Methods 62 317–26
- [45] Cheng J, Sheldon E L, Wu L, Heller M J and O'Connell J P 1998 Isolation of cultured cervical carcinoma cells mixed with peripheral blood cells on a bioelectronic chip *Anal. Chem.* 70 2321–6
- [46] Lagally E T, Lee S-H and Soh H T 2005 Integrated microsystem for dielectrophoretic cell concentration and genetic detection Lab Chip 5 1053–8
- [47] Oh K W, Park C, Namkoong K, Kim J, Ock K-S, Kim S, Kim Y-A, Cho Y-K and Ko C 2005 World-to-chip microfluidic interface with built-in valves for multichamber chip-based PCR assays *Lab Chip.* 5 845–50
- [48] Chen R W, Piiparinen H, Seppanen M, Koskela P, Sarna S and Lappalainen M 2001 Real-time PCR for detection and quantitation of hepatitis B virus DNA J. Med. Virol. 65 250–6